AJP

ISSN : 0971 - 3093

Vol 25, No 7, July, 2016

ASIAN JOURNAL OF PHYSICS

An International Research Journal

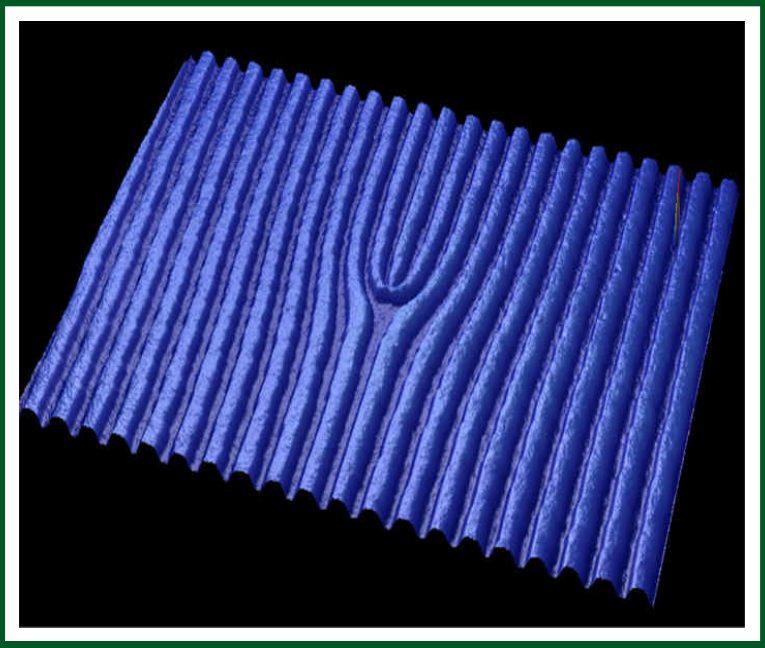

ANITA PUBLICATIONS

FF-43, 1st Floor, Mangal Bazar, Laxmi Nagar, Delhi-110 092, India

B O : 2, Pasha Court, Williamsville, New York-14221-1776, USA

Asian Journal of Physics
Vol. 25, No 7 (2016) 809-831
Available on: www.asianjournalofphysics.in

Graphene: A review of optical properties and photonic applications

M K Kavitha and Manu Jaiswal
Department of Physics, Indian Institute of Technology Madras, Chennai-600 036, India

This article gives a brief overview of the broad-range optical response of graphene and its scope for photonic applications. The optical absorption of single-layer graphene is unique, since it is governed entirely by a fundamental constant of nature, the fine structure constant. The absence of frequency dependence or a dependence on any material properties are noteworthy characteristics. The origin of the optical properties of graphene is discussed with regard to its peculiar band structure and the massless relativistic nature of its charge carriers. Electrostatic gating is one useful knob to modulate the optical absorption, since it modifies the position of the Fermi energy in this low-dimensional material. The experimental evaluation of the optical response of graphene using spectroscopic ellipsometry is discussed in detail. Reduced graphene oxide is the defective counterpart of graphene that can be solution-processed. Its optical properties can be varied by tuning the size of sp^2-rich graphene domains. The optical properties of defected graphene are discussed and the important contribution of confined two-dimensional water present in the interlayers is also highlighted. Finally, interesting photonic applications in photodetectors, non-linear optical elements and photovoltaics arising from the combination of unique electronic and optical properties of graphene and its derivatives are summarized.

Keywords: Graphene, Fine-structure constant, Electrostatic gating, Spectroscopic Ellipsometry, Non-linear optics

1 Introduction

Graphene is a monolayer of sp^2-hybridized carbon atoms arranged in a honeycomb lattice. The hybridized orbitals form strong σ-bonds in the plane and un-hybridized p-orbitals overlap with neighboring atoms to form π-bond. While the σ-bond is responsible for the most of the structural integrity of graphene, the π-bond determines electronic and optical properties. The interaction of graphene with electromagnetic radiation is fascinating due to the two-dimensional confinement of electrons and the exceptional band structure of graphene. Graphene has a simple band structure with zero band-gap, but its optical response is non-trivial. In this review article, we provide a description of the mechanism of broadband optical absorption in graphene, together with applications that are based on these optical properties. The band structure of graphene consists of completely filled conduction band and empty valence band which cross linearly at the Dirac point [1]. The optical absorption of pristine graphene is attributed to the interband and intraband transitions. For single-layer graphene, absorption in the visible spectral region is negligibly small and also frequency independent [2]. However, this "negligibly small" absorption must be seen in light of the single-atom thickness of the absorbing layer. With this thickness is taken into account, it is not difficult to see that the light-matter interaction in graphene is rather extraordinarily large. On substrates with low roughness, graphene can be visualized under white light illumination, despite being a single atom thick layer [3]. The Femi-level can be easily tuned by electrostatic gating or equivalently by electron/hole chemical doping, which brings about large control over its optical properties [4]. In the far infrared region absorption can be explained within a Drude model [5] and it can be tuned over a broad terahertz frequency range by tailoring

Corresponding author :
e-mail: manu.jaiswal@iitm.ac.in, Phone: 044 22574893 (Manu Jaiswal)

graphene nanostructures and electrostatic gating [6]. When illuminated with ordinary light, the photogenerated charge carriers thermalize, and subsequently cool down non-radiativelyto form a non-equilibrium distribution near the Dirac point, this gives rise to hot luminescence [7]. When it is illuminated with ultra-short laser pulses, larger concentrations of thermalized electrons are obtained and this saturates further absorption of light due to Pauli blocking [8]. The above discussion mainly pertains to pristine graphene which has a high degree of perfection in the atomic lattice. Structural defects in the lattice produced during the growth and processing steps, modify its electronic properties and consequently also influence the optical properties. High quality graphene can be synthesized by different techniques like mechanical exfoliation or by chemical vapor deposition (CVD). Graphene obtained from each method possesses distinct optical properties due to the structural defects. For example, CVD graphene is characterized by small densities of sp3-defects, besides line defects at the grain boundaries [9]. Furthermore, CVD graphene contains some amount of amorphous carbon and polymeric residue and metal catalyst impurities. While these physisorbed impurities usually have a minimal impact on the electrical properties, they can lead to artifacts in the measured optical response. The band structure and mechanisms of optical transitions in defected graphene are also discussed in this review article, with particular reference to reduced graphene oxide. Spectroscopic ellipsometry is illustrated as a tool to probe the optical constants of graphene and graphene oxide. Finally, we discuss how the optical properties in graphene are useful towards several photonic applications.

2 Band structure of graphene

Graphene has a honeycomb crystal lattice network of sp^2 hybridized carbon atoms. The honeycomb lattice can be viewed as interpenetrating triangular lattice with a basis of two atoms per unit cell, labelled as A and B. The view from point B is rotated by 180 degrees as compared to the view from point A. The Bravais lattice is also triangular and it consists of two atoms per unit cell, as represented in Fig1a with lattice vectors $a_1 = \frac{a}{2}(3,\sqrt{3})$ and $a_2 = \frac{a}{2}(3,-\sqrt{3})$, Where a is the nearest neighbor Carbon-Carbon spacing (≈0.142 nm). The reciprocal lattice is also triangular with lattice vectors, $b_1 = \frac{2\pi}{3a}(1,\sqrt{3})$ and $b_2 = \frac{2\pi}{3a}(1,-\sqrt{3})$. The first Brillouin zone (BZ) of the reciprocal lattice is also a honeycomb lattice, but it is rotated by an angle of π/2 with respect to the real space lattice, as shown in Fig 1b. The six corners of the first BZ consist of two set of inequivalent points, **K** and **K′**, these are called the Dirac points [1]. In the band structure of graphene, σ-states form occupied and empty states with a wide energy gap, while the π-states form a single band with conical self-crossing point in the **K** points (and similarly in **K′** points).The structure of electronic energy bands and Brillouin zones is developed using tight bound approximation considering the hopping of electrons in the plane of honeycomb lattice [10]. The energy band derived from tight-binding Hamiltonian is given by Eq (1), where t is nearest neighbor hopping energy and t' is the next nearest hopping energy. Reich *et al* estimated the first three hopping parameters, namely $t = -2.8$ eV, $t' = -0.33$ eV and $t'' = -0.073$ eV by *ab initio* calculations [11]. Figure 2a shows the full band structure of graphene. The hopping energy to next nearest neighbors diminishes with distance in the lattice and energy dispersion spectrum is symmetric around the Dirac point. The Fermi-level coincides with the Dirac point, where the completely filled valence band and the empty conduction band meet with zero band-gap. Figure 2b clearly illustrates that energy bands near to the Dirac points are linear and it also reveals that graphene is a semimetal, i.e. a zero band-gap semiconductor. This linear dispersion is applicable only up to an energy of ~ 1 eV, and the charge carriers in this region behave like relativistic massless Fermions, obeying Dirac equation [12]. Thus in the vicinity of Dirac point, energy dispersion relation is isotropic and form a Dirac cone. Moving away from Dirac cone, trigonal wrapping initially modifies the energy contours, further there is a saddle point (**M**-point) in the energy bands and at the **Γ**-point the energy bands are widely separated.

$$E_{\pm}(\boldsymbol{k}) = \pm t\sqrt{(3 + f(k)} - t' f(k), f(\boldsymbol{k}) = 2\cos(\sqrt{3}\,k_y a) + 4\cos\left(\frac{\sqrt{3}}{2}k_y a\right)\cos\left(\frac{3}{2}k_y a\right) \quad (1)$$

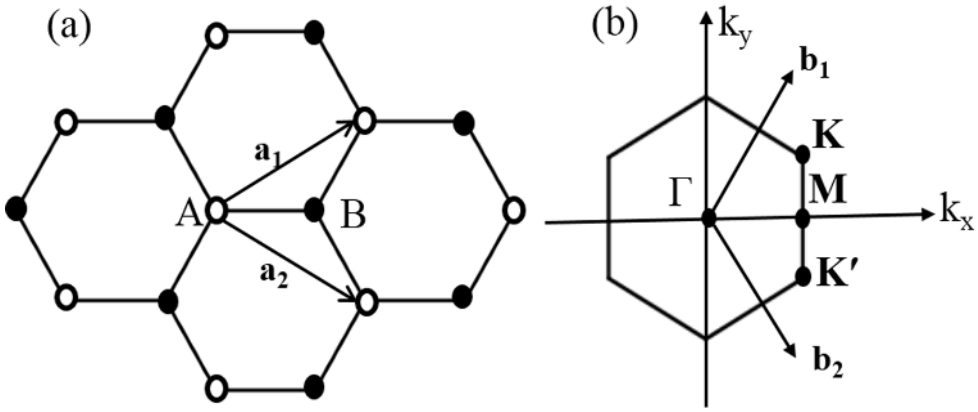

Fig 1. (a) Honeycomb lattice structure of graphene. The unit cell consists of carbon atoms represented by A and B, $\mathbf{a}_1$ and $\mathbf{a}_2$ are the lattice vectors and (b) corresponding Brillouin zone, showing the high-symmetry points.

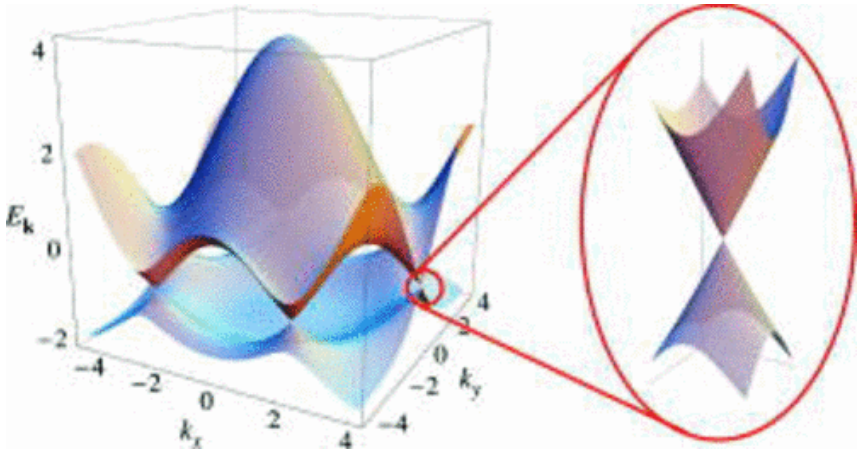

Fig 2. (a) Electronic dispersion for the honeycomb lattice. (b) Band structure near the Dirac point. "Reprinted (Fig 3) with permission from [1]. © (2009) by the American Physical Society."

The electronic dispersion near the Dirac point in the hexagonal BZ is $\boldsymbol{E} = \pm \hbar v_F |\mathbf{q}|$, where v_F is the Fermi velocity of the carriers, with a value of $\approx 10^6$ m/s (about c/300, where c is the velocity of light) and $\mathbf{q}$ is the k-vector measured relative to the **K**-point. The two dimensional density of states (DOS) over the Brillouin zone is obtained by performing the integral, $D(E) = \frac{1}{2\pi^2} \int (E(\mathbf{k}) - E) d^2k$ [13]. The resulting DOS consists of van Hove singularities (VHS) at the saddle points (or **M** points) in the band structure. While applying the Dirac approximation, $E = \pm \hbar v_F \mathbf{q}$, the final expression for DOS in the low-energy region becomes $D(E) = 2|E| / \pi\hbar^2 v_F^2$. The DOS of graphene is different from the DOS of carbon nanotubes, thelatter shows typical characteristics of one-dimensional systems with $1/\sqrt{E}$ dependence, in contrast with linear dependence of single-layer graphene and constant value for other 2D electron gases [14]. In graphene, the VHS is widely separated, far away from the Fermi level and it is difficult to access by varying gate voltage and doping [14]. Hence, the charge transport experiments do not typically probe these high energy regions [15]. The discussion so far pertains to pristine single-layer graphene. We next consider the bilayers and multilayer

graphene. In bilayer and few layer graphene, the layers are stacked in different ways namely, hexagonal or AA-stacking, Bernal or AB-stacking and rhombohedral or ABC-stacking. These are formed in nature with varying abundance and exfoliated graphene obtained from natural graphite usually comprises of a mixture of variously stacked graphene. The band structure in these systems arises from the coupling of different monolayers. In bilayer graphene, electrons have finite mass and band structure consists of pair of hyperbolic bands. Bilayer graphene is also zero band-gap material but the pair of valence band and conduction bands are separated by interlayer hopping of electrons [16]. Finally, it should be noted that graphene layers with random orientations of successive layers can also be artificially assembled and the positions of the VHS can be significantly altered in these cases [17].

3 Preparation of graphene

The most common techniques for making graphene include chemical vapor deposition (CVD) [18-21], exfoliation methods [22], epitaxial growth [23-25] and graphene oxide reduction [26]. The quality, size and number of layers of graphene sheets obtained vary from one method to another. Novoselov *et al* had first shown micromechanical cleavage of graphite to yield single- and few-layer graphene [22]. Today, graphene flakes up to 1mm size can be obtained by micromechanical or dry exfoliation methods. For mechanical exfoliation, either high-quality natural graphite or highly oriented pyrolytic graphite (HOPG) is transferred to a scotch tape, which is then used to peel off graphitic layers onto a substrate. This process is very reliable and gives the highest quality graphene with charge carrier mobilities up to a million cm^2/Vs at room temperature. However, this process has extremely low yield and it suited only for laboratory scale research experiments. High-quality graphene can be deposited on metal substrates such as nickel and copper by CVD at ambient or low pressures using a carbon source like camphor, methane, propane etc [27]. Growth on polycrystalline nickel films give monolayer and few layer graphene while single crystalline Ni gives predominantly monolayer graphene [18]. Because of low solubility of carbon in Cu, it is a better catalyst for the growth of monolayer graphene. CVD technique can be used to make wafer-scale single-layer graphene and few-layer graphene at a low-cost and it can be transferred from the metal surface to desired substrates through polymer assisted methods [21]. Transfer-free epitaxial growth of graphene is also possible by heating silicon carbide (SiC) in vacuum or inert atmosphere [23]. The electronic properties of resulting graphene depends whether SiC surface had carbon or silicon atom termination prior to the growth. On the Si-face, homogeneous clean graphene can be grown with a controlled number of layers while on the C-face, although the number of layers is not homogeneous, twisted bilayer graphene can be grown [23]. The lateral dimensions of graphene films obtained by this method can be greater than 50 μm but the yield is generally poor [23]. Graphene can also be formed by unzipping carbon nanotubes. This can be done in solution phase by the action of potassium permanganate and sulfuric acid or by plasma etching of CNTs embedded in a polymer [28, 29]. This method has high yield and graphene nanoribbons of few μm size can be easily obtained. Graphene nanoribbons are semiconducting with a non-zero band-gap due to the additional confinement of ribbon geometry and also due to edge-disorder. Another low-cost method to prepare graphene is by reduction of graphene oxide (GO) [30, 31]. GO solution can be obtained by treating graphite with strong oxidizers followed by exfoliation. Thin films can be drop-cast or spin-coated from the solution, which can subsequently be reduced by thermal or chemical methods to obtain graphene. The quality of the film obtained by this process is low because of the presence of oxygen functional groups and defects even after the reduction is done; however this process is highly scalable and suited for industrial applications. Figure 3 shows the optical image of graphene prepared by mechanical exfoliation, CVD grown graphene transferred to Si/SiO_2 substrate and rGO films on Si/SiO_2 substrate. Graphene made by each of these methods have been found suitable for specific applications.

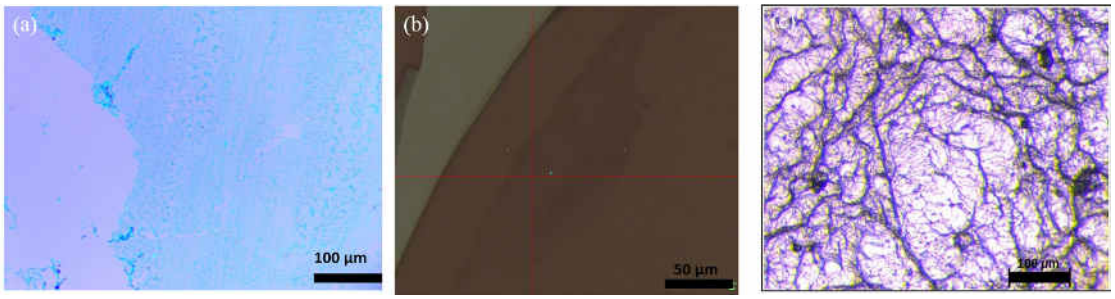

Fig 3. Optical image of (a) CVD grown on copper and transferred to Si/SiO_2 (b) mechanically exfoliated graphene (c) reduced graphene oxide on Si/SiO_2 prepared by thermal annealing of GO.

4 Optical transitions in graphene

The optical properties of graphene become unique on account of the linear band structure, zero band-gap and strong interaction of Dirac Fermions with electromagnetic radiation. Graphene absorbs over a wide spectral range, and this is contributed from interband and intraband optical transitions. The absorption of graphene from visible to near infrared region is modeled by interband transitions and it is frequency independent, described by fine structure constant [2, 32]. The optical response in far infrared region is due to the intraband transitions or free carrier absorption [33]. Direct photon absorption is not possible by intraband transition due to the momentum mismatch. To conserve momentum, phonon scattering occurs, followed by a population inversion of free carriers near the **K**-point. The conductivity from free carrier absorption shows a Drude like frequency dependence [5]. The far infrared response can be tuned to terahertz range by plasmonic excitations of charge carriers [6]. Plasmon assisted light absorption is not allowed in graphene because of the large momentum mismatch between the photons and plasmons [34]. However, plasmon excitations can be activated by electrostatic gate coupling and engineering graphene nanostructures [35]. Ju *et al* have demonstrated that plasmon frequency enhances with decreasing the size of graphene nanoribbons [6].

5 Frequency-independent absorption of graphene in visible wavelength region

Generally in solids, the atoms are closely packed and their outer atomic orbitals strongly overlap each other. This interaction broadens the discrete levels and they form bands. The electronic states in these bands are delocalized, and optical transitions are possible between them. The interband transitions are possible over a range of photon energies, depending on the position of upper and lower bands. For example, silver absorbs ultraviolet photons and reflects all visible and infrared wavelengths. The ultraviolet frequency coincides with an electron jumping from valence band comprising of filled 3d-orbitals to unoccupied states of 4s-orbitals. This is generally observed in all metals. Gold also could be expected to absorbs ultraviolet frequency associated with the electronic transition from 5d to 6s orbital. But in gold, the 6s electrons get closer to the nucleus than does the 5d electrons. This provides a significant velocity to the electron in the 6s orbital, whose value is comparable to the speed of light. In other words, 6s valence electrons in gold are relativistic particles when compared to electrons of lighter elements. This is why a gold atom shifts the frequency enough to put it in the visible color range while a silver atom does not. Thus gold would be silver in color without relativistic effect [36, 37]. Thus special theory of relativity plays an important role in determining the color of metals. Relativity also appears as a key phenomenon in context of the optical properties of graphene. This is discussed in the following paragraph.

Graphene is a zero-gap material with linear energy dispersion, conduction band and valence band touch at this Dirac point, as shown in Fig 2b. The energy dispersion near the Dirac point is linear, such

that the electrons and holes in the background of a honeycomb lattice mimic relativistic particles that are described by the Dirac relativistic equation. Graphene exhibits a particularly unique but simple optical absorption spectrum. In the infrared-to-visible spectral range, its absorbance has been calculated to be not only independent of the frequency of the electromagnetic radiation, but it is also independent of any material properties of the absorber! The absorbance of suspended single-layer graphene is defined by the fine structure constant as $\pi\alpha$, where $\alpha = e^2/\hbar c$ is the fine-structure constant [2]. The fine structure constant is a dimensionless number, with a value 1/137 and it has intrigued every physicist from Arthur Eddington, Wolfgang Pauli to Max Born. Feynman has remarked the following about the fine structure constant, "It's one of the greatest damn mysteries of physics: a magic number that comes to us with no understanding by man" [38]. So what has this fine structure constant to do with the optical transmission of graphene? The origin of the optical properties being defined by this fundamental fine structure constant lies in the two-dimensional relativistic nature of charge carriers in graphene, as discussed below.

The excitation near the Dirac point is governed by linear wave vector (k) dependent energy dispersion, $E_k = \hbar v_F |k|$, where $v_F = 10^6$ m/s, is the Fermi velocity. When light wave with electric field component ($\bar{E}$) and frequency (ω) is incident perpendicular to a sheet of graphene, the incident energy can be estimated as, $W_i = \frac{c}{4\pi} |\bar{E}|^2$. The absorption can be estimated within time-dependent perturbation theory, treating the sinusoidal electromagnetic potentials within a semiclassical approximation. The interaction between electromagnetic radiation and charge carriers in graphene is described by the Hamiltonian, $\hat{H} = v_F \vec{\sigma} \cdot \left(\hat{p} - \frac{e}{c}\vec{A}\right) = \widehat{H_0} + \widehat{H_{int}}$, here the first term is the standard Hamiltonian for quasiparticles in graphene and the second term describes their interaction with electromagnetic field [2]. According to Fermi's golden rule, energy absorbed W_a is given by Eq (2):

$$W_a = \frac{2\pi}{\hbar} |M|^2 D(E_k - E_l)\hbar\omega \tag{2}$$

where D is the density of states at half the energy of incident radiation, $E_k = E/2 = \hbar\omega/2$. For $2D$ Dirac fermions in graphene, $D(\hbar\omega/2) = \hbar\omega/\pi\hbar^2 v_F^2$, a linear function of E_k. M is the matrix element for the interaction of Dirac fermions in graphene with electric field component and it is given by Eq (3) [2].

$$|M|^2 = |\langle f| v_F \vec{\sigma} \cdot \frac{e}{i\omega}\bar{E}|i\rangle|^2 = \frac{1}{8} e^2 v_F^2 \frac{|E|^2}{\omega^2} \tag{3}$$

The percentage of energy absorbed is given as $W_a / W_i = \pi(e^2/\hbar c) = \pi\alpha = 2.3\%$. Therefore, the optical absorption is independent of incident frequency and material parameters. The amount of light passing through graphene can therefore be used as a simple means to estimate the fine-structure constant or the Planck's constant. Figure 5a shows the optical image of an aperture partially covered by monolayer and bilayer graphene and Fig 5b represents transmittance measured under illumination [2]. When graphene is illuminated with white light, the monolayer region absorbs 2.3 %, with negligible reflectance < 0.01 %. The absorption is found to increase with graphene thickness such that each layer adds another 2.3 % to amount of absorbed radiation. There is an interesting analogy of this result with the phenomenon of planetary motion, as described within Newtonian mechanics. The Kepler's third law of planetary motion states that R^3/T^2 is a constant for the planet orbiting the sun, where R is the natural length scale and T is the natural time scale of the problem. This constant value happens to be independent of the initial conditions of the problem, because the angular momentum cancels out in the ratio. In a similar vein, Heinz *et al*. have explained purelyon the basis of dimensional analysis, that the Hamiltonian of graphene describing linear band structures lacks an intrinsic energy scale with which the photon energy can be compared [34]. It follows that the Fermi velocity and the frequency do not appear in the expression for optical transmission of graphene. The relativistic nature

of carriers in graphene is therefore at the heart of the explanation why the optical transmission is simply given by π times the fine structure constant. The electronic properties of graphene can be significantly modulated with lattice strain [39]. The polarization-dependent optical response of graphene also contains signatures of lattice strain-induced changes in the band structure of graphene, which can be directly monitored in a transmission experiment [40].

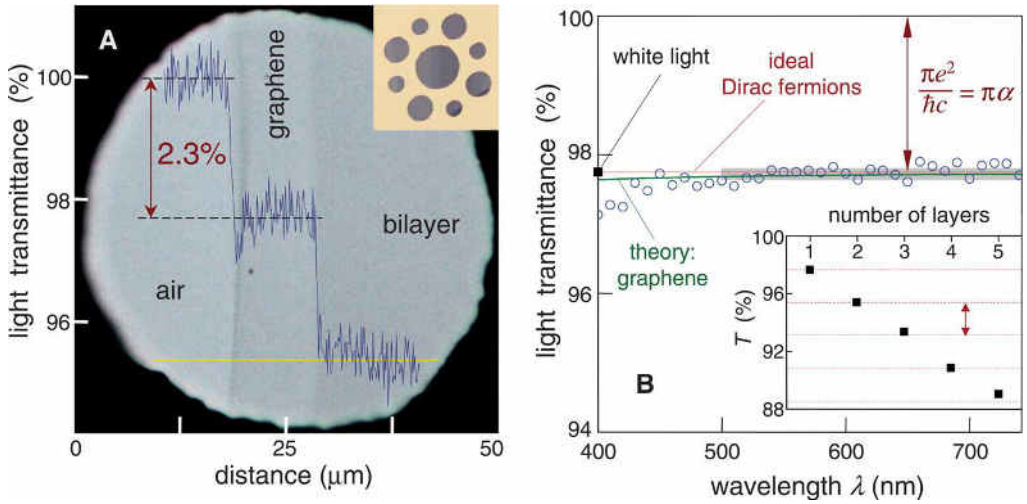

Fig 4. (a) Photograph of a 50 μm aperture covered by graphene and its bilayer. Inset- sample design: A 20 μm thick metal support structure having several apertures of 20, 30 and 50 μm in diameter with graphene crystallites placed over them. (b) Transmittance of single layer graphene. Inset- transmission of white light as a function of the number of graphene layers. "From [2]. Reprinted with permission from AAAS".

6 Gate dependent optical transitions

External electric-field modulated conductivity is the basis of modern electronics. For low-dimensional materials, an external electric field shifts position of the Fermi level, resulting in change in the electric current. Similar to the knob on electrical current, a gate voltage can also serve as a knob on optical transmission of low-dimensional systems. Unlike other materials, a large modification of optical transition by electric field gating is observed in graphene [4]. This type of optical transition modulation has also been reported in carbon nanotubes, but the underlying mechanism is different because of the difference in electronic band structure [41, 42]. The extent of optical transparency of carbon nanotubes depends on whether they are metallic or semiconducting in nature, because of the difference in the energy positions of the van Hove singularities in the DOS, as shown in Fig 5a. Since the DOS associated with the van Hove singularities is very high, the associated optical absorption is also very high. The gap energies between the van Hove singularities in conduction band and valence band of metallic and semiconducting nanotubes are ≥ 2.5 eV and ≤ 1 eV, respectively [43]. So transparency modulation with electric field is easily accessible in metallic nanotubes due to the easily available van Hove singularities. Jaiswal *et al* described the IR transparency modulation with gating in a semiconductor enriched SWNT network [41, 44]. The SWNT network was prepared by spray coating on to a heated glass slide. Figure 5b shows the schematic of the field-effect device that comprises of an electrolyte gate in contact with SWNT electrodes that are separated by a narrow gap. The optical absorption in the IR region through one of the SWNT electrodes is given in Fig 5c and the modulated absorption in semiconductor sample is due to the prominent S_{11} absorption. The Fermi level in SWNT is positioned close to one of the van Hove singularities prior to application of the electric-field. The external electric-field shifts

the Fermi level following the formation of a charged double layer at the SWNT: electrolyte interface. This results in the depletion of electrons from the van Hove singularity and consequent increase in free carrier absorption [41].

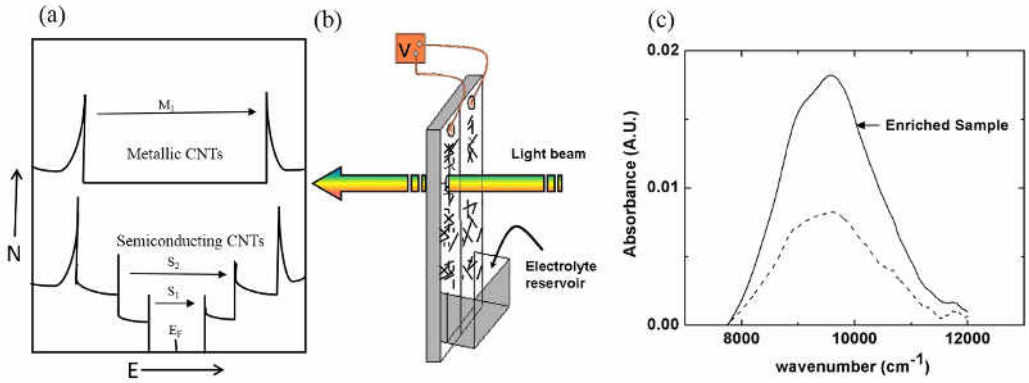

Fig 5. (a) Density of states of metallic and semiconducting carbon nanotubes (b) Schematic of field effect device with electrolyte gating (c) Spectral absorbance of SWNT network device [44].

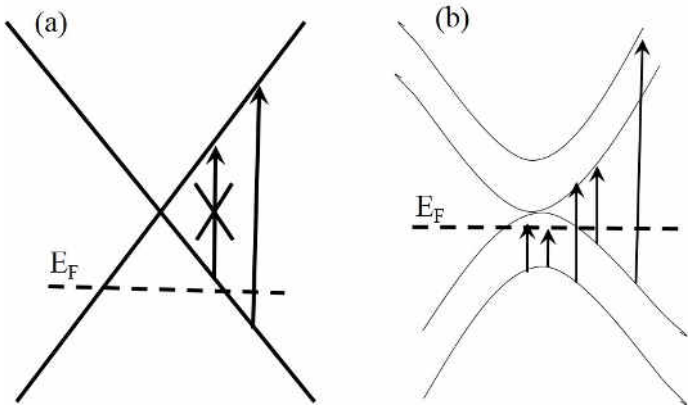

Fig 6. Gate tunable interband transitions in (a) monolayer (b) bilayer graphene

In graphene, since the van Hove singularities are situated far away from the Fermi level, they are inaccessible for experiments involving gate-modulated optical transmission [1]. In this system, field-effect modulated optical transition can be related to the exceptionally low density of states near Dirac point. This low DOS causes significant shift in Fermi energy with variation in carrier density [4]. The IR absorption in pristine graphene is strictly a universal constant since the linear energy dispersion in graphene holds up to 1 eV energy, as discussed earlier. The applied gate voltage shifts the Fermi energy E_F, where $E_F = \pm n\hbar v_F$, where 'n' is the charge carrier density which depends on the applied gate voltage [4]. Such electrostatic doping strongly changes the interband absorption through Pauli blocking. The interband transitions for photon energy $< 2E_F$ are blocked for hole-doped graphene while those with photon energy $> 2E_F$ remain unaffected, as schematically represented in Fig 6a. This significantly modulates the IR absorption, such that there is an increase in absorption corresponding to the shift in Fermi level. The gate induced IR absorption

in bilayer graphene is significantly different from that of monolayer because of the difference in electronic band structure. In hole-doped bilayer graphene, the optical transitions between pair of valence bands are allowed and a strong emission is related to the van Hove singularity [4]. With the increase in hole doping, the emission becomes more prominent due to the down shift of E_F and more transitions are possible, as given in Fig 6b. A small band-gap will also appear in bilayer graphene because of the asymmetry of the applied electric field on the bilayers [45]. This tunability of IR response in monolayer graphene and bilayer graphene using an applied external gate voltage holds potential for the development of novel graphene base tunable photodetectors.

7 Structure and optical properties of graphene oxide

Graphene oxide (GO) is a chemically-modified graphene generated from graphite oxide. Graphene oxide (GO) is a chemically-modified graphene generated from oxidation of graphite, typically using Brodie's or Hummer's method [46-49]. GO consists of single or few-layer graphite oxide obtained from the colloidal dispersion of graphite oxide in water and other organic solvents. GO has a highly disordered structure. The poor electrical conductivity is due to the presence of several oxygen functional groups mainly hydroxyls and epoxy on basal plane and small amount of carboxyls, carbonyls and lactones at the edges, which scatter the charge carriers in graphene [50-52]. Figure 7a shows the structure of graphene oxide. The presence of these oxygen-rich functional groups also renders some benefits for using GO in the fabrication of opto-electronic devices [53]. The oxygen functional groups makes GO hydrophilic such that it forms stable dispersions in polar solvents which is used as a precursor for the synthesis of graphene. The stable dispersions of GO can be deposited on any hydrophilic surface. Figure 7b shows the IR spectrum of GO, the most prominent band is in the range of 3000–3700 cm^{-1} and is due to the stretching modes of adsorbed/intercalated H_2O, along with hydroxyls and carboxyls. The other vibrational modes in GO correspond to oxygen functionalities like ketonic species (1650–1750 cm^{-1}), carboxyls (1600–1650 cm^{-1}), asymmetric vibrational stretching of C=C along with H_2O bending modes (1500-1600 cm^{-1}) and epoxides (1230-1320 cm^{-1} and ~850 cm^{-1}). The region of spectral overlap (850–1500 cm^{-1}) is broken down into three regions namely α region (900–1100 cm^{-1}) for all ether derivatives, β region (1100–1280 cm^{-1}) for ketonic species along with peroxides, pyran and γ region (1280–1500 cm^{-1}) for epoxides. GO sheets consist of tetrahedral sp^3 carbon atoms where the oxygen groups are attached interspersed with unoxidised graphitic region with sp^2 carbon atoms as shown in Fig 7a.

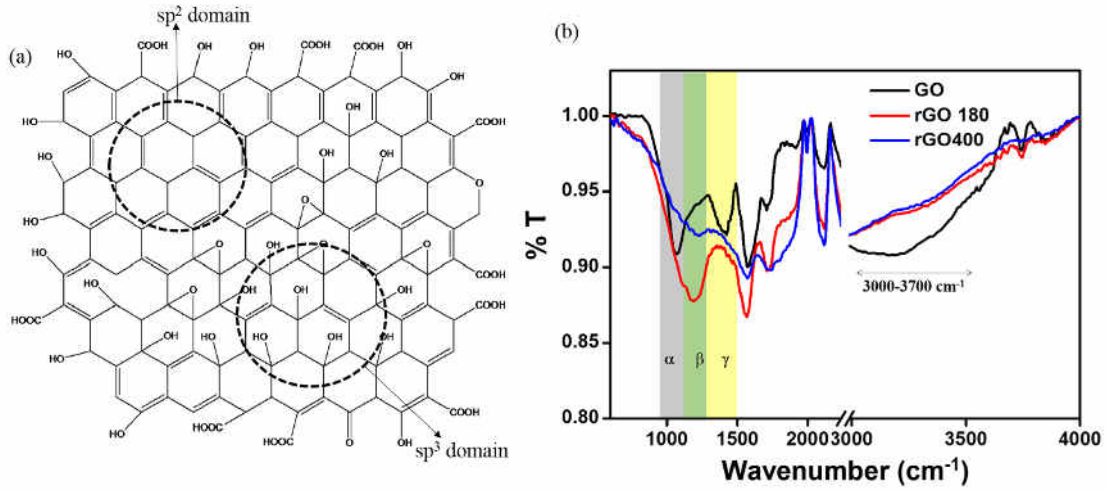

Fig 7. (a) Structure of graphene oxide representing sp^2 and sp^3 domains (b) IR spectrum of graphene oxide, rGO-180 and rGO-400.

The versatility of GO is that its disordered structure can be partly converted to graphene like sheets by removing the functional groups and restoring the conjugated structure. Typical GO films are insulating with wide energy gap in the density of states and sheet conductivity of the order of 10^{12} Ω/sq. or more [50, 54, 55]. The reduction of solution processed GO films can be done by thermal annealing in vacuum or inert gas atmosphere, by exposure to hydrazine vapor or sodium borohydride or by laser heating [56-60].The structure of reduced graphene oxide (rGO) is described as graphitic islands of nanometer size separated by oxidized graphene. This random distribution of graphitic domain and oxidized sp^3 domain, breaks the symmetry and opens a band-gap in rGO. The band-gap is a transport gap, since there are intervening regions of mid-gap states [61, 62].The optical response of rGO depends on the size of graphitic domains and the coverage of oxygen functional groups. Shen *et al* experimentally investigated the optical absorption of rGO from IR to ultraviolet region [63]. The optical absorption in IR and visible region is approximately 2.5 to 3.5 %, which is similar to the absorption of graphene layer. There is prominent peak in ultraviolet region, which is shifted from 5.1 to 4.5 eV depending on the reduction level of rGO [63]. Theoretical studies have predicted that there is linear decrease in the bandgap with decrease in the oxygen content of GO. Ultraviolet absorption in rGO is due to π to π* transitions, its value lies between 4.8 eV and 5.2 eV when the coverage of oxygen functional groups is 25 % and 75 %, respectively [64]. Carbonyl groups are mainly responsible for the shift in π plasmon peak [64]. In unreduced GO, hydroxyl and epoxy groups are prominent with small amount of carbonyls groups, while in rGO the concentration of carbonyl groups increases. The increase in carbonyl groups creates a vacancy in the graphene sheet and an increase in the vacancies leads to the tearing of graphene sheets and decrease in band-gap with respect to that of functionalized graphene [61, 64]. Acik *et al* have experimentally demonstrated this carbonyl formation in rGO by IR spectroscopic studies [65]. In Fig 4b, the IR spectra of GO and rGO annealed at 180°C (denoted as rGO-180) is compared. Thermal annealing results in a regular decrease in the intensity of vibrational modes in the range of 3000–3700 cm^{-1} owing to the removal of hydroxyls and adsorbed/intercalated H_2O water molecules from GO. For rGO-180, the water modes completely disappear while the oxygen-containing species are still retained. The vibrational peak corresponding to the ketonic region (1650–1750 cm^{-1}) is slightly increased, suggesting the formation of carbonyls during the removal of hydroxyls by a free radical reaction. The trapped water between the adjacent layers of GO will dramatically influence the chemistry of multilayer GO upon mild thermal annealing up to 200 °C [66]. Water molecules are confined in the interlayer nanospacing of multilayered GO. These confined water will assist the formation of defects and carbonyl groups in multilayer graphene. Further annealing to 400 °C, will remove the oxygen functional groups and trapped water, resulting in defective graphene structures (Fig 7b). The electronic and optical properties of GO can tuned by controlling the reduction and the trapped water. This aspect is discussed in more detail in a subsequent section of this article.

8 Experimental determination of optical constants: spectroscopic ellipsometry

Spectroscopic ellipsometry (SE) can be applied to evaluate the optical properties of graphene and graphene oxide from ultraviolet to infrared spectral region [67-74]. Ellipsometry is a non-destructive optical measurement based on the principle that light undergoes change in polarization as it reflects from the surface of the sample or after passing through layered optical media. The polarization states of incident and reflected light wave are described by the orthogonal components of electric field namely p- and s- polarization, as shown in Fig 8. The component parallel to the plane of incidence is called 'p-polarized' and that which is perpendicular to the plane of incidence is called 's-polarized'. After reflection from the surface the amplitude and phase of p- and s- polarized states change in such a way that it becomes elliptically polarized. Ellipsometry measures two parameters, denoted as amplitude ratio (Ψ) and phase difference (Δ) between the p- and s-polarizations, respectively and it is related to the ratio of amplitude reflection coefficients (ρ) as shown in equation $\rho = \tan\psi \exp(i\Delta)$ [75].

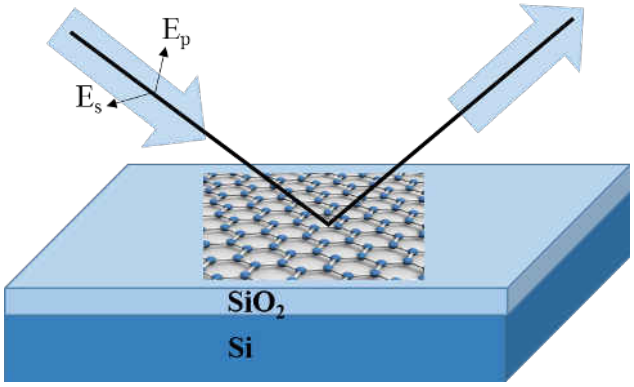

Fig 8. Schematic diagram of graphene positioned on SiO_2/Si substrate for ellipsometric measurements.

The wavelength dependent optical constants (n, k) and/or the thickness of the film can be extracted from Ψ and Δ by formulating an optical dispersion model for the sample. Optical constants of the material are related to its dielectric function ϵ by the equation, $\epsilon^2 = n + i\,k$. This complex dielectric function describes both the electric polarization and the absorption properties of the material and it is represented by a complex function $\epsilon_1 \pm i\,\epsilon_2$. The dielectric function spectra contains unique fingerprints of electronic properties and band structure of materials, where imaginary part ϵ_2 is most directly related to the interband transitions [13]. Furthermore, ϵ_1 and ϵ_2 depend on each other through the well-known Kramers-Kronig (KK) relation, as shown in Eq (4) [76].

$$\epsilon_1 = 1 + \frac{2}{\pi} P \int_0^{\infty} \frac{\omega' \epsilon_2(\omega')}{\omega'^2 - \omega^2} \tag{4}$$

where P denote the principle value of integral and ω' is the complex angular frequency. To extract the optical parameters of the material from the (Ψ, Δ) spectra, the dielectric function of the material has to be modeled. There are many dielectric function models, we need to select an appropriate model according to the type of the material i.e. depending on if it is transparent or absorbing in nature. For the transparent region, a Cauchy model is often used, while free carrier absorption can be studied within a Drude model [76]. The B-spline layer is used for partially transparent and partially absorbing materials. To express the electric polarization in the visible/UV region, various models including the Lorentz model, Tauc–Lorentz model, harmonic oscillator approximation (HOA), and modeldielectric function (MDF) have been used [76]. Basically, all these models are derived from the Lorentz model. The Lorentz model is a classical model which describes electric polarization in terms of a negatively-charged electron being bound to a positively-charged atomic nucleus with a spring. When electromagnetic wave is incident onto the sample, the electric-field will induce polarization in the material such that motion of electrons can be described by oscillator models. The dielectric function of electronic oscillators can be represented by Lorentz model by Eq (5):

$$\epsilon(\lambda) = \epsilon_{\infty} + \sum_i \frac{A_i}{E_i^2 + (\frac{hc}{\lambda})^2 - iB_i(\frac{hc}{\lambda})} \tag{5}$$

where $\epsilon(\lambda)$ is the dielectric constant, i is the number of oscillators, A_i is the amplitude, E_i is the center energy and B_i is the broadening of the oscillator for the i^{th} oscillator, respectively. Since optical constants and electronic transitions in the material are related to dielectric constant, these can be directly extracted from the ellipsometric data. This capability of spectroscopic ellipsometry can be utilized to elucidate the optical absorption of graphene, and further, to unravel its unique electronic spectra. For probing the samples, generally the spot sizes for collimated beam of SE is crucial and it is assumed that the film characteristics are reasonably uniform within this spot size region. The minimal size of an ellipsometric spot is about 50 μm or

more in a focused beam ellipsometer, while it can be higher (300 μm) in a conventional system. However, it is quite challenging to produce such sufficiently large graphene flakes using mechanical exfoliation on a flat dielectric substrate in order to measure the ellipsometric data in a wide spectral range. Isić *et al* used an island film model to extract the optical constants with an error of 10 % since size of a typical few-layer graphene flake is actually smaller than ellipsometric spot size [70]. This problem can be addressed by using a spatially-resolved imaging ellipsometer with a spot-size less than 1μm [77, 78]. Kravets *et al* were successful in obtaining graphene flakes of size (200 × 200) μm^2, which is large enough to measure using the focused beam of an ellipsometer [68]. It is not easy to define a precise optical thickness of an atom-thin layer. In literature, the optical constants are often modeled by fixing the thickness of graphene as 0.335 nm, which is the expected interlayer spacing in graphite or the size of the π-electron cloud in graphene. It must however be noted that the optical thickness of graphene as obtained from best fit values varies from flake to flake and this cannot be easily rationalized [68, 69].

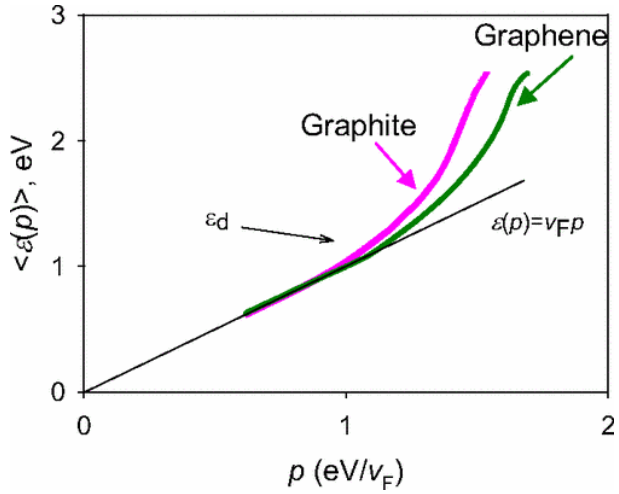

Fig 9. Exciton dispersion relation in graphite and graphene at low energy calculated from the respective optical transmission spectra. "Reprinted (Fig 1) with permission from [68] Copyright (2010)by the American Physical Society".

As discussed earlier, the optical absorption of graphene in the visible region is governed by the fine structure constant. Kravets *et al* [68] represented its low energy electronic spectrum from the optical absorption by a simple relation, given in Eq (6), where W is the absorbed energy of incident light per unit area calculated by the Fermi golden rule, W_0 is the total energy incident on the system, g is the degeneracy of states and $\varepsilon(p)$ is the eigenvalue of the graphene Hamiltonian. This expression can be generalized for any 2D system with a symmetric electronic spectrum. The electronic dispersion relations for graphite and graphene can be arrived at from this expression, as shown in Fig 9. At low energy excitations, the electronic spectrum demonstrates the behavior of mass Dirac fermions with linear dispersion and slope deviates from linear dependence and give an estimate of nearest neighbor hopping energy, $t \approx 2.9$ eV [1].

$$Abs(\omega) = \frac{W}{W_0} = \frac{g\pi\alpha}{2}\left[n(-\varepsilon) - n(\varepsilon)\right]\frac{dln(\varepsilon)}{dln(p)}\Big|_{\varepsilon = \hbar\omega/2} \tag{6}$$

For ellipsometric measurements, high quality graphene flake is exfoliated on SiO_2/Si substrate and light is incident on the sample at variable angles, as shown in Fig 8. The optical spectra obtained is then fitted with a multilayer model consisting of silicon, silicon dioxide, a Cauchy layer (consisting of water/ air trapped in between substrate and graphene) and graphene. The optical constants are deduced from the

ellipsometric data and are used to calculate the absorption spectra for graphene and graphite. Yang *et al* theoretically predicted the optical response of graphene, bilayer graphene and graphite with and without excitonic resonant effects, as plotted in Fig 10 [79]. Absorption spectra have a peak at 4.6 eV, it is due to the van Hove singularities in the density of states and excitonic effects [68, 74, 78]. They found that in the ultraviolet region, absorption grows rapidly to give a peak at 5.1 eV due to the van Hove singularity and it is down shifted by 600 meV. This downshift is attributed to excitonic resonance effects, as shown in Fig 10a. This exciton-induced downshift was experimentally verified by Kravets *et al* [68]. The optical absorption in IR region slightly increases with wavelength since it also has contributions from plasmonic excitations associated with free carriers [5, 74].

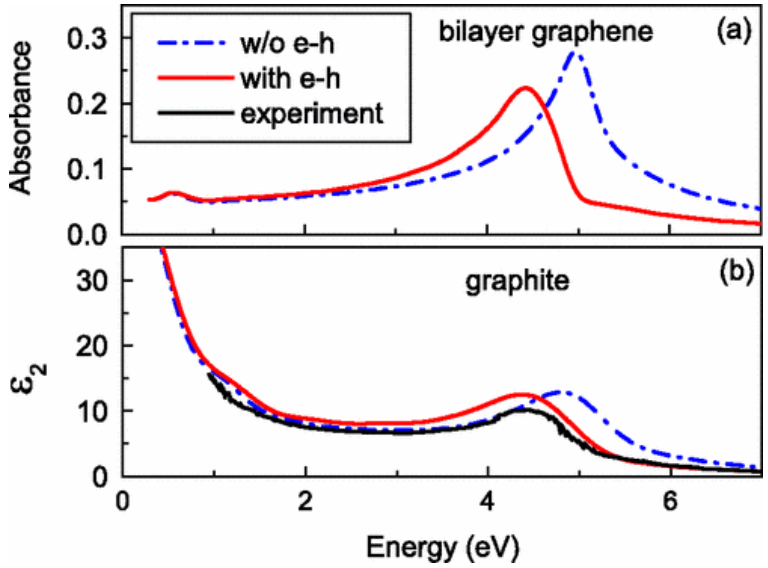

Fig 10. (a) Absorbance of bilayer graphene and (b) imaginary part of the dielectric function of graphite, with and without excitonic effects included "Reprinted (Fig 4) with permission from [79] Copyright (2009) by the American Physical Society".

Spectroscopic ellipsometry can also be used to determine the optical response of disordered graphene systems such as graphene oxide and reduced graphene oxide. [72, 73, 80]. In this case, it is non-trivial to draw inferences on the energy bands, in a manner similar to the case of pristine graphene crystals. Shen *et al* [73] described a three layer model of substrate SiO_2/GO/air to analyze the ellipsometric parameters GO and few-layer rGO. Lorenz oscillator model was used to to arrive at quantitative estimates of the band energy distribution. The optical response of rGO in the visible wavelength region is similar to that of graphene and the reduction in bandgap tuning following elimination of oxygen-rich groups can be inferred from the ellipsometric data [73]. In this and several other previous works , the role of trapped water has not been considered while analyzing the optical properties of GO. Ghosh *et al* [72] demonstrated that trapped monolayers of water between the GO layers primarily govern the changes of refractive index of GO as it is successively reduced in a controlled manner, rather than the chemical structure changes of GO. The important observation was that the optical constants of the composite GO: water system estimated from spectroscopic ellipsometry change rather abruptly between 125 - 160 ^{o}C annealing temperatures. This abrupt change in refractive index in the narrow annealing temperature interval can potentially be due to two factors namely (i) abrupt change in the chemical structure of GO or (ii) expulsion of trapped water. This temperature coincides

with the elimination of water from the system as seen from IR studies (Fig 7b). At the same time, the IR studies as well as Raman studies [51] indicate that the chemical structure of GO changes rather minimally in this annealing temperature interval. It is therefore natural to associate the large changes in refractive index of GO upon its thermal reduction to the elimination of trapped interfacial water. Further evidence supporting this idea stems from the estimates of interlayer separation of GO flakes as the system undergoes thermal annealing. An X-ray diffraction (XRD) plot of GO samples shows a prominent peak at 11.5^{o} which correspond to a c-axis separation (d) of 7.8 Å, small peak at 27^{o} corresponding to graphitic carbon. Table 1 show the peak position and d-spacing for GO and rGO samples at different annealing temperatures. After thermal annealing at varying temperature, peak at 11.5^{o} shifts to higher angle with a decrease in d-spacing to 6.6 Å (T = 150 ^{o}C) because of the removal of oxygen functional groups and trapped water. Further annealing above 160 ^{o}C, graphitic peak becomes prominent and peak at 11.5^{o} is absent. Previous molecular dynamics (MD) calculations have indicated that trapped water will form continuous monolayer layer of water, if d ≥ 6 Å [81]. Figure 11 represents frequency dependent refractive index for GO and differently annealed rGO samples. For samples annealed at temperatures ≥ 180 ^{o}C, the refractive index approaches that of graphite. Significant change in the value of refractive index occurs in the temperature interval of 125-160 ^{o}C [72].

Table 1. Peak position and d-spacing of GO and rGO annealed at different temperature

Sample	XRD Peak Position (degree)	d spacing (Å)
GO	11.54	7.7
r GO-100	11.84	7.5
r GO-125	12.1	7.2
r GO-140	12.6	7.0
r GO-150	13.49	6.6

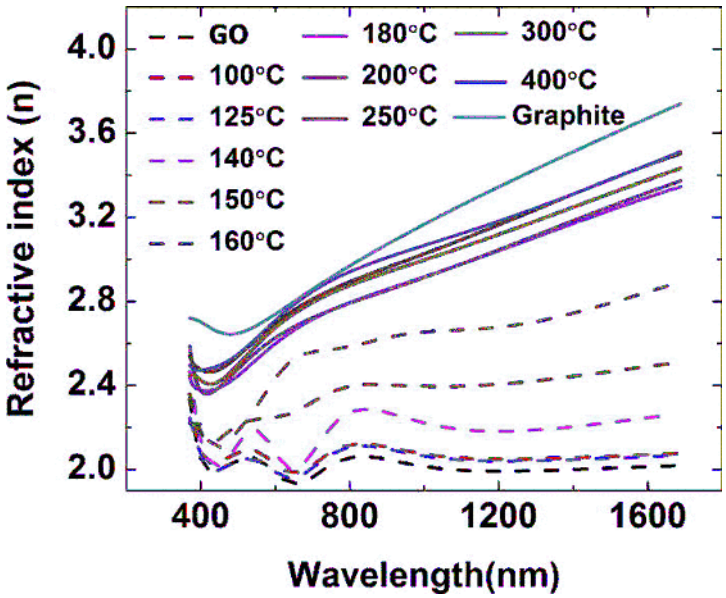

Fig 11. Refractive index vs wavelength of as-prepared GO and GO annealed at different temperatures. Reprinted (Fig 2) with permission from [72]. © [2015], AIP Publishing LLC.

The importance of this experiment lies not only in the fact that it gives the correct origin of the refractive index of GO films, but also because GO is an ideal system to probe two-dimensional water. The interlayer separations in GO can be tuned such that a monolayer of water can be either present or they can be eliminated. The hydrogen bonding network and density of two-dimensional water are predicted to be different from that bulk water and this subject has not been explored [82]. Recently, a new form of ice, the square ice, has been discovered in water trapped between graphene layers [83], though the existence of this square lattice has also been subsequently disputed [84, 85]. In this context, ellipsometry can be a useful tool to study the properties of water confined between graphene and graphene-oxide layers. In this section, we have provided a thorough account of the use of spectroscopic ellipsometry to investigate the optical properties of graphene and disordered graphene. In the next section, we consider how graphene can be optically visualized on different substrates.

9 Image processing and optical contrast

It is challenging to visualize mechanically exfoliated single and few-layer graphene on an arbitrary substrate because of extremely low yield and lack of sufficient optical contrast between graphene and the substrate, and also between graphene layers of different thickness. Single-layer graphene can however be readily visualized under an optical microscope using a substrate of appropriate optical constants and thickness, such as a 300 nm thick SiO_2/Si wafer [22]. The optical visibility of monolayer and bilayer graphene is due to the contrast between graphene and dielectric oxide layer on the substrate and the visibility is much stronger in reflectance than in transmission [86]. Visualization of graphene is possible by the strong amplitude modulation at the air-graphene-SiO_2 interface [87]. Blake *et al* experimentally demonstrated a dependence of contrast on the thickness of the oxide layer on silicon and probing wavelength based on Fresnel's Law [3]. For a certain thickness of SiO_2, even a single layer of graphene will give sufficient contrast to distinguish it from thicker

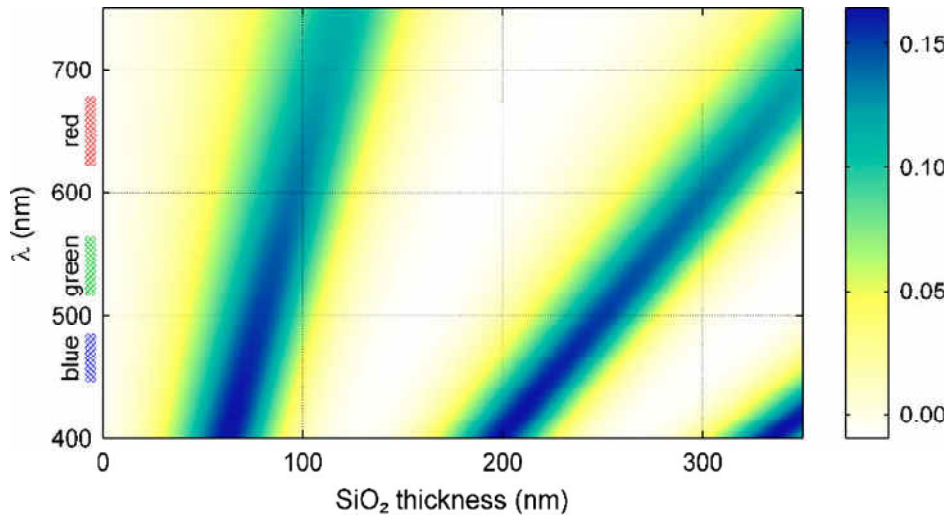

Fig 12. Color plot of the expected contrast as a function of wavelength and thickness of SiO_2. "Reprinted (Fig 3) with permission from [3]. © [2007], AIP Publishing LLC".

flakes over. Contrast is defined as the relative intensities of reflected light in presence and absence of graphene on the dielectric layer. Single layer graphene gives maximum contrast of 12 % for any given wavelength and SiO_2 thickness [3]. The opacity of graphene is also an important factor determining the contrast, so it can be used as a quantitative tool to define the number of layers. This model can be extended to find graphene crystallites on any substrate like poly methyl methacrylate (PMMA), silicon nitride etc. Under white light

illumination, single layer graphene on Si wafer with standard thickness of 300 nm SiO_2 is visible, but it is invisible on top of 200 nm SiO_2. By using narrow band filters graphene is visible on any thickness of SiO_2 except for 150 nm and below 30 nm. Figure 12 shows a color plot of contrast as a function of wavelength and SiO_2 thickness. It is useful in selecting filters appropriate for a given thickness of SiO_2.

We next consider the visualization of graphene on polymeric substrates. For example, single-layer graphene deposited on polydimethylsiloxane (PDMS) has a positive value of contrast with an absolute value much smaller than what is observed in case of SiO_2 /Si substrate. However, the average magnitude of contrast can be made comparable to that of graphene on SiO_2/Si system, if we use few-layer graphene (e.g. two or three layers). This initially suggests that we might actually see few layer graphene on PDMS. Practically this is not realized. The explanation lies in the fact that the contrast is a rapidly oscillating function of both the thickness of the polymer and the wavelength of light. It follows that small variations in the thickness of the polymer can lead to a rapid contrast change and these can be greater than the contrast arising from few layer graphene. This prevents visualization of few-layer graphene on a substrate like PDMS [88].

10 Photoluminescence

Since graphene lacks an electronic bandgap, photoluminescence (PL) is not possible from relaxed charge carriers. But in single-layer pristine graphene significant light emission is observed under excitation by near infrared (1.5 eV) femtosecond laser pulses [7]. The light emission is found to occur in the entire spectral region from 1.7 eV to 3.5 eV. Since the light emission occurs well above the incident photon energy and its nonlinear dependence on laser input fluence rules out the possibility of conventional hot-emission from non-thermalised electrons. These observations can be understood within the framework of a thermal emission model. Femtosecond excitations produce carriers of transient temperature above 3000 K, which give rise emission in the visible region. But for a continuous wave excitation with same pumping energy, the emission in this spectral region is not observed for pristine graphene. This type of PL by non-thermalized electrons can be induced in graphene by creating an energy band-gap by chemical functionalization [89]. The chemical method involves functionalization of graphene sheets or cutting it into smaller sheets such that it forms quantum confined sp^2 islands with structural defects [90-93]. These structural defects will play a critical role in band-gap opening and electronic emission. Chemically modified graphene derivatives namely graphene oxide and reduced graphene oxide show wide spectral photoluminescence from ultraviolet to near infrared region. As- prepared GO solution exhibits broad emission with predominant peak in yellow region. Radiative recombination of electron-hole pairs in sp^2 domains are responsible for ultraviolet and blue luminescence in rGO [90, 93]. As described in a previous section, GO consists of a mixture of sp^2 and sp^3 domains, and its optical properties are determined by the π-π^* transitions from the sp^2 sites. As-prepared GO contains a large fraction of distorted carbon atoms with oxygen functional groups which induces localization of the otherwise delocalized π-states. These localized states are responsible for the higher wavelength optical emission of GO. When GO is reduced to rGO, the concentration of disordered carbon atom reduces, resulting in a blue shift in the photoluminescence spectra [91]. Thus PL in GO and rGO can be controlled by the size of sp^2 clusters and the concentration of oxygen functional groups. Another relayed system is that of graphene quantum dots (GQDs), which are small fragments of graphene sheets confined in three dimensional space with size less than 20 nm [92, 94, 95]. GQDs have non-zero band-gap and shows photoluminescence due to quantum confinement effects and edge effects [92, 96]. Functionalized GQDs exhibit a red shift in PL emission when compared to unfunctionalized GQDs because of charge transfer between the functional groups [96].

11 Photonic applications

Graphene and its derivatives interact with electromagnetic radiation from ultraviolet to terahertz region. Such broadband interaction with light and unique electronic properties makes graphene a promising candidate for photonic applications. Graphene has high electrical conductivity and a large transmission

value, which suggests that it can be used as transparent conductor for many photonic devices like flat panel displays, solar cell and light emitting devices [21, 97, 98]. Currently indium tin oxide (ITO) and fluorine doped tin oxide (FTO) are the commercially used transparent electrodes because of their low sheet resistance of 10-25 Ω/sq. and transmittance above 90 % [99]. In contrast to ITO or FTO, graphene is light weight, mechanically flexible, chemical stable and can be synthesized with low-cost techniques. Graphene can be prepared by several methods such as mechanical exfoliation, epitaxial growth and chemical vapor deposition. All these methods limit the mass production of graphene in a required area of substrate. Bae *et al* succeeded in a roll-to-roll production of 30 inch monolayer graphene film by chemical vapor deposition method [21]. These graphene film have sheet resistance less than 125 Ω/sq. and optical transmittance above 95 % and these have been incorporated in a touch screen panel device which can withstand high strain. Considerable efforts have been made to create reduced graphene oxide based transparent electrodes. Stable transparent rGO films can be prepared by spray coating, spin coating, dip coating and vacuum filtration [30, 55, 100-102]. Thermally annealed spin-coated and spray-coated rGO films give resistance less than 1 kΩ/sq. with greater than 80 % light transmittance from visible to far infrared region [55]. Ultra-thin films can be prepared by vacuum filtration of GO dispersions through cellulose acetate membrane. It can be transferred to any flexible substrate by dissolving the membrane and further chemical treatment gives rGO films. Transparency of these rGO films can be tuned from 65 % to 95 % and sheet resistance can be reduced by several orders of magnitude, makes it good candidate for transparent flexible electrodes [30].

There are versatile applications of graphene in photovoltaic devices, such as a flexible transparent electrode, photosensitized material and a charge transporting layer. Wang *et al* demonstrated transparent, conductive ultrathin graphene films as an alternative to ITO window electrode for solid-state dye-sensitized solar cells (DSSCs) [97]. The TiO_2 layer captures the photoexcited electrons from the dye molecules in DSSCs. Graphene materials are incorporated in TiO_2 scaffold to improve the photocurrent density by enhanced electron transport, dye adsorption and light scattering [103-105]. Graphene or its composites with metals, conducting polymers or other carboneous materials can be used as substitute for platinum as counter electrode in DSSCs [106-109]. Perovskite solar cells (PSCs) are promising third generation solar cells. Graphene derivatives have excellent conductivity and very high charge extraction rate. Therefore, their use in PSCs can help to enhance the performance of these solar cells. Wang *et al* [97] achieved one of the highest efficiencies in mesostructured perovskite solar cell by utilizing graphene as the charge collection layer. They employed low temperature processed nanocomposite of graphene and TiO_2 as electron collection layer with reduced series resistance and recombination losses [110]. Yan *et al* successfully assembled the multilayer graphene/perovskite interface as Schottky junction, which surpasses spiro-OMeTAD (hole conducting layer) in hole extraction rate [111, 112]. In making transparent or semi-transparent PSCs, a replacement of Au/Ag back contact with transparent electrodes is required. You *et al* presented a semi-transparent PSC using graphene electrodes with efficiency over 10% when illuminated from both sides [113] and this suggests scope of using PSCs as tandem cells to silicon solar cells [114]. Metal oxide transparent electrodes are used as anode for organic light emitting diodes (OLEDs). Since these metal oxides form poor electrical contact with organic materials, it is among the major bottleneck in the fabrication of efficient OLEDs. The compatibility of graphene and rGO makes it suitable for promising next generation transparent anode in OLEDs if it can fulfill the required sheet resistance and optical transmittance [115-117]. When graphene is used as cathode layer in OLEDs, the electron injection from cathode to organic layer is reduced due to its high work function. In order to use as an effective cathode layer, the work function of graphene is reduced by n-doping. Thus with n-doped graphene cathode, solution processed OLEDs can be fabricated [118].

Ultra-high bandwidth photodetectors can be fabricated with single and multilayer graphene, from ultraviolet to terahertz region. Photodetection depends on the conversion of absorbed photons to electrical signal. In pristine graphene, because of strong electron-electron interaction, photoexcited electron will undergo ultrafast heating in the order of femtoseconds. Photogenerated hot electrons produce photovoltage

by a photothermoelectric effect at much faster time scale [119]. If an external electric field is applied, the charge carriers get separated and photocurrent is generated because of photovoltaic effect. This type of field can be generated internally near metal-graphene interfaces and it can be used for ultrafast photoresponse in graphene. Metal-graphene-metal photodetectors are the first class of graphene based photodetectors that have been demonstrated [120, 121]. External doping or electrostatic gate voltage has been applied to improve the photoresponse [122]. Metal contacts near the graphene channel in graphene based photo detectors further improves the response since localized plasmons in metal contacts will cause field enhancement [123].

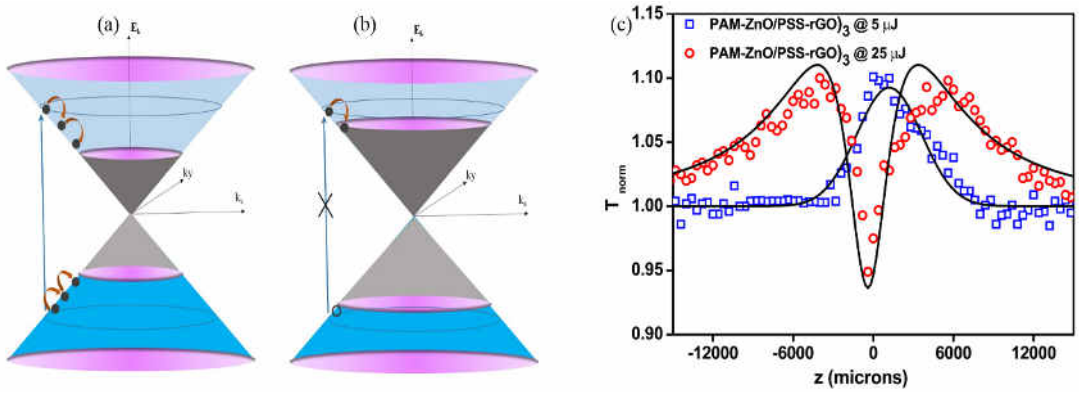

Fig 13. Schematic representation of interband transition in graphene (a) the photogererated carriers produces non-equilibrium population of hot carriers in valence and conduction band (b) For high enough intensity excitations, the photogenerated carriers fill the conduction and valence band, which results in Pauli blocking (c) Switching of absorption from saturable to reverse saturable in ZnO/graphene hybrid films [136].

Ultra-fast carrier dynamics related to the linear dispersion of Dirac electrons, the broad band light absorption and Pauli blocking together makes graphene an ideal nonlinear optical material. Materials with nonlinear optical property are used in photonic applications like laser manufacturing, optical switches, mode-locking and optical limiting. Interband transitions by ultra-short pulses, produces non-equilibrium population of hot carriers in valence and conduction bands. Two types of relaxations are possible for these hot carriers: (i) ultrafast relaxations in the order of femtoseconds by carrier interband collisions and photoemission (ii) picosecond timescale relaxations corresponding to an interband relaxation and cooling of hot electrons. After photoexcitation and relaxation in sub-picosecond timescale, a Fermi-Dirac distribution of carriers forms near the Dirac point as shown in Fig 13a. This distribution of charge carriers reduces the further absorption of photons by Pauli blocking and results in the phenomena of saturable absorption as given Fig 13b. This can further be modulated by varying the number of layers of graphene. Graphene saturable absorbers can be integrated in laser systems for the generation of ultra-short pulses [8, 124-127]. Graphene materials also show reverse saturable absorption (RSA), involving an increase in absorption with increase in the input laser energy. Such materials can be used as optical limiters, which possess high transmittance for low incident light intensity and low transmittance for high intensity. This occurs due to the nonlinear scattering by the formation of solvent bubbles in dispersion and carbon microplasma [128]. Optical limiters are used to protect eye and other sensors from high radiation visible to far IR region. Conventional optical limiting materials are phthalocyanines, ZnO, PbS, carbon nanotubes and fullerenes [128-132]. To further improve the optical limiting property, different hybrids of graphene with the above materials have been considered [133-135]. Switching of nonlinear absorption is possible in these hybrid materials, depending on the energy of incident radiation and it can be measured by open aperture z-scan technique. Figure 13c shows the switching of nonlinear absorption from saturable to reverse saturable in ZnO/graphene hybrid films [136]. This switching of nonlinear absorption in this self-assembled ZnO/graphene films can be

demonstrated as follows. When the film is far away from the focus, the input intensity is too low to induce nonlinearity and the transmittance is unity. When the film is moved further near to the focus, the intensity of light falling on the sample is increased and the ground state gets depleted causing saturable absorption, so that the transmittance increases. On the other hand as the film reaches the focus, still higher intensities are seen by the film and reverse saturable absorption dominates, causing strong optical limiting. Hence, transmittance decreases effectively and falls to a value less than unity. Thus graphene films and its composites are promising candidates for nonlinear optical applications.

12 Conclusions

The Dirac Fermions in graphene have amongst the strongest light-matter interactions known for any system, with an optical transmission that is governed by the fine structure constant. The pristine graphene system is valuable test-bed for table-top studies on the foundations of physics. On the other hand, the optical properties of graphene are also widely tunable either by means of electrical gate-modulation or by the presence of defects, by quantum confinement effects and due to the presence of interfacial water layers. In this work, the basic optical properties of graphene and its derivatives are discussed, together with the existing and potential applications of this unique system.

References

1. Castro Neto A H, Guinea F, Peres N M R, Novoselov K S, Geim A K, *Rev Mod Phys*, 81(2009)109-162.
2. Nair R R, Blake P, Grigorenko A N, Novoselov K S, Booth T J, Stauber T, Peres N M R, Geim A K, *Science*, 320(2008)1308; doi: 10.1126/science.1156965
3. Blake P, Hill E W, Castro Neto A H, Novoselov K S, Jiang D, Yang R, Booth T J, Geim A K, *Appl Phys Lett*, 91(2007)063124; doi.org/10.1063/1.2768624.
4. Wang F, Zhang Y, Tian C, Girit C, Zettl A, Crommie M, Shen Y R, *Science*, 320(2008)206-209.
5. Horng J, Chen Chi-Fan, Geng Baisong, Girit Caglar, Zhang Yuanbo, Hao Zhao, Bechtel Hans A, Martin Michael, Zettl Alex, Crommie Michael F, Shen Y Ron, Wang Feng, *Phys Rev B*, 83(2011)165113; doi.org/10.1103/PhysRevB.83.165113
6. Ju L, Geng B, Horng J, Girit C, Martin M, Hao Z, Bechte Hans A, Liang X, Zettl A, Shen Y. Ron, Wang F, *Nat Nano*, 6(2011)630-634.
7. Lui C H, Mak K F, Shan J, Heinz T F, *Phys Rev Lett*, 105(2010)127404; doi.org/10.1103/PhysRevLett.105.127404.
8. Bao Q, Zhang H, Wang Y, Ni Z, Yan Y, Shen Z X, Loh K P, Tang D Y, *Adv Funct Mater*, 19(2009)3077-3083.
9. Lijin G, Aparna G, Shaina P R, Nandita Das G, Manu J, *Nanotechnology*, 26(2015)495701; doi:10.1088/0957-4484/26/49/495701.
10. Wallace P R, *Phys Rev*, 71(1947)622-634.
11. Reich S, Maultzsch J, Thomsen C, Ordejón P, *Phys Rev B*, 66(2002)035412; doi.org/10.1103/PhysRevB.66.035412.
12. Novoselov K S, Geim A K, Morozov S V, Jiang D, Katsnelson M I, Grigorieva I V, Dubonos S V, Firsov A A, *Nature*, 438(2005)197-200.
13. Kittel C, Introduction to Solid State Physics, 7th Edn, (Wiley), 1996.
14. Mintmire J W, White C T, *Phys Rev Lett*, 81(1998)2506-2509.
15. Pachoud A, Jaiswal M, Ang P K, Loh K P, Özyilmaz B, *Europhys Lett*, 92(2010)27001; doi:10.1209/0295-5075/92/27001.
16. McCann E, Abergel D S L, Fal'ko V I, *Eur Phys J Spec Top*, 148(2007)91; doi:10.1140/epjst/e2007-00229-1.
17. George L, Jaiswal M, ICC-2015, Bikaner, (2016) *AIP Conference*; doi.org/10.1063/1.4946370.
18. Yu Q, Lian J, Siriponglert S, Li H, Chen Y P, Pei S S, *Appl Phys Lett*, 93(2008)113103; doi.org/10.1063/1.2982585.

19. Guermoune A, Chari T, Popescu F, Sabri S S, Guillemette J, Skulason H S, Szkopek T, Siaj M, *Carbon*, 49(2011) 4204-4210.
20. Strudwick A J, Weber N E, Schwab M G, Kettner M, Weitz R T, Wünsch J R, Müllen K, Sachdev H, *ACS Nano*, 9(2015)31-42.
21. Bae S, Kim H, Lee Y, Xu X, Park Jae-Sung, Zheng Y, Balakrishnan J, Lei T, Kim H R, Song Y I, Kim Y-J, Kim K S, Özyilmaz B, Ahn J-H, Hong B H, Iijima S, *Nat Nano*, 5(2010)574-578.
22. Novoselov K S, Geim A K, Morozov S V, Jiang D, Zhang Y, Dubonos S V, Grigorieva I V, Firsov A A, *Science*, 306(2004) 666-669.
23. Norimatsu W, Kusunoki M, *Phys Chem Chem Phys*, 16(2014)3501-3511.
24. Pallecchi E, Lafont F, Cavaliere V, Schopfer F, Mailly D, Poirier W, Ouerghi A, *Sci Rep*, 4(2014)4558; doi:10.1038/srep04558.
25. Riedl C, Coletti C, Starke U, *J Phys D Appl Phys*, 43(2010)374009; doi:10.1088/0022-3727/43/37/374009.
26. Pei S, Cheng H M, *Carbon*, 50(2012)3210-3228.
27. Somani P R, Somani S P, Umeno M, *Chem Phys Lett*, 430(2006)56-59.
28. Kosynkin D V, Higginbotham A L, Sinitskii A, Lomeda J R, Dimiev A, Price B K, Tour J M, *Nature*, 458(2009) 872-876.
29. Jiao L, Zhang L, Wang X, Diankov G, Dai H, *Nature*, 458(2009)877-880.
30. Eda G, Fanchini G, Chhowalla M, *Nat Nano*, 3(2008)270-274.
31. Stankovich S, Dikin D A, Piner R D, Kohlhaas K A, Kleinhammes A, Jia Y, Wu Y, Nguyen S T, Ruoff R S, *Carbon*, 45(2007)1558-1565.
32. Mak K F, Sfeir M Y, Wu Y, Lui C H, Misewich J A, Heinz T F, *Phys Rev Lett*, 101(2008)196405; doi.org/10.1103/PhysRevLett.101.196405.
33. Gierz I, Petersen J C, Mitrano M, Cacho C, Turcu I C E, Springate E, Stöhr A, Köhler A, Starke U, Cavalleri A, *Nat Mater*, 12(2013)1119-1124.
34. Mak K F, Ju L, Wang F, Heinz T F, *Solid State Commun*, 152(2012)1341-1349.
35. Kim J, Son H, Cho D J, Geng B, Regan W, Shi S, Kim K, Zettl A, Shen Y R, Wang F, *Nano Lett*, 12(2012)5598-5602.
36. Pyykko P, Desclaux J P, *Acc Chem Res*, 12(1979)276-281.
37. Christensen N E, Seraphin B O, *Phys Rev B*, 4(1971)3321-3344.
38. Feynman R P, QED: The Strange Theory of Light and Matter. (Princeton University Press ISBN 0-691-08388-6) 1985.
39. Shaina P R, Jaiswal M, *Appl Phys Lett*, 105(2014)193103; doi.org/10.1063/1.4901746.
40. Ni G X, Yang H Z, Ji W, Baeck S, Toh C T, Ahn J H, Pereira V M, Özyilmaz B, *Adv Mater*, 26(2014)1081-1086.
41. Jaiswal M, Sangeeth C S, Wang W, Sun Y P, R M, *J Nanosci Nanotechnol*, 9(2009)6533-6537.
42. Weisman R B, Bachilo S M, *Nano Lett*, 3(2003)1235-1238.
43. Kataura H, Kumazawa Y, Maniwa Y, Umezu I, Suzuki S, Ohtsuka Y, Achiba Y, *Synthetic Metals*, 103(1999)2555-2558.
44. Jaiswal M, Ph D Thesis, Charge transport in transparent single-wall carbon nanotube networks and devices, Indian Institute of Science, Bangalore, India, 2008.
45. Mak K F, Lui C H, Shan J, Heinz T F, *Phys Rev Lett*, 102(2009)256405; doi.org/10.1103/PhysRevLett.102.256405.
46. Brodie B, *Ann Chim Phys*, 59(1860)466-472.
47. Staudenmaier L, *Ber Dtsch Chem Ges*, 31(1898)1481-1487.
48. Hummers W S, Offeman R E, *J Am Chem Soc*, 80(1958)1339-1339.
49. Marcano D C, Kosynkin D V, Berlin J M, Sinitskii A, Sun Z, Slesarev A, Alemany L B, Lu W, Tour J M, *ACS Nano*, 4(2010)4806-4814.

50. Eda G, Chhowalla M, *Adv Mater*, 22(2010)2392-2415.
51. Kajen R S, Chandrasekhar N, Pey K L, Vijila C, Jaiswal M, Saravanan S, Ng A M H, Wong C P, Loh K P, *J Appl Phys*, 113(2013)063710; doi.org/10.1063/1.4792042
52. Eda G, Mattevi C, Yamaguchi H, Kim H, Chhowalla M, *J Phys Chem C*, 113(2009)15768-15771.
53. Loh K P, Bao Q, Eda G, Chhowalla M, *Nat Chem*, 2(2010)1015-1024.
54. Gómez-Navarro C, Weitz R T, Bittner A M, Scolari M, Mews A, Burghard M, Kern K, *Nano Lett*, 7(2007)3499-3503.
55. Becerril H A, Mao J, Liu Z, Stoltenberg R M, Bao Z, Chen Y, *ACS Nano*, 2(2008)463-470.
56. Park S, An J, Potts J R, Velamakanni A, Murali S, Ruoff R S, *Carbon,* 49(2011)3019 3023.
57. Shin H J, Kim K K, Benayad A, Yoon Seon-Mi, Park H K, Jung I-S, Jin M H, Jeong H-K, Kim J M, Choi J-Y, Lee Y H Lee, *Adv Funct Mater*, 19(2009)1987-1992.
58. Tao Y, Varghese B, Jaiswal M, Wang S, Zhang Z, Oezyilmaz B, Loh K P, Tok E S, Sow C H, *Appl Phys A*, 106(2011)523-3023.
59. Zhou Y, Bao Q, Varghese B, Tang L A L, Tan C K, Sow C-H, Loh K P, *Adv Mater*, 22(2010)67-71.
60. El-Kady M F, Kaner R B, *Nat Commun*, 4(2013)1475; doi:10.1038/ncomms2446.
61. Boukhvalov D W, Katsnelson M I, *J Am Chem Soc*, 130(2008)10697-10701.
62. Pereira V M, Lopes dos Santos J M B, Castro Neto A H, *Phys Rev B*, 77(2008)115109; doi.org/10.1103/PhysRevB.77.115109
63. Shen Y, Yang S, Zhou P, Sun Q, Wang P, Wan L, Li J, Chen L, Wang X, Ding S, Zhang D W, *Carbon*, 62(2013)157-164.
64. Johari P, Shenoy V B, *ACS Nano*, 5(2011)7640-7647.
65. Acik M, Lee G, Mattevi C, Pirkle A, Wallace R M, Chhowalla M, Cho K, Chabal Y, *J Phys Chem C*, 115(2011) 19761-19781.
66. Acik M, Mattevi C, Gong C, Lee G, Cho K, Chhowalla M, Chabal Y J, *ACS Nano*, 4(2010)5861-5868.
67. Weber J W, Calado V E, van de Sanden M C M, *Appl Phys Lett*, 97(2010)091904; doi.org/10.1063/1.3475393.
68. Kravets V G, Grigorenko A N, Nair R R, Blake P, Anissimova S, Novoselov K S, Geim A K, *Phys Rev B*, 81(2010) 155413; doi.org/10.1103/PhysRevB.81.155413.
69. Losurdo M, Giangregorio M M, Bianco G V, Capezzuto P, Bruno G, *Thin Solid Films*, 571(2014)389-394.
70. Isić G, Jakovljević M, Filipović M, Jovanović D, Vasić B, Lazović S, Puač N, Petrović Z L, Kostić R, Gajić R, Humlíček J, Losurdo M, Bruno G, Bergmair I, Hingerl K,, *J Nanophotonics*, 5(2011)051809-.; doi:10.1117/1.3598162.
71. Li W, Cheng G, Liang Y, Tian B, Liang X, Peng L, Hight Walker A R, Gundlach D J, Nguyen N V, *Carbon*, 99(2016)348-353.
72. Ghosh M, Pradipkanti L, Rai V, Satapathy D K, Vayalamkuzhi P, Jaiswal M, *Appl Phys Lett*, 106(2015)241902; doi.org/10.1063/1.492273.
73. Shen Y, Zhou P, Sun Q Q, Wan L, Li J, Chen L Y, Zhang D W, Wang X B, *Appl Phys Lett*, 99(2011)141911; doi.org/10.1063/1.3646908.
74. Nelson F J, Kamineni V K, Zhang T, Comfort E S, Lee J U, Diebold A C, *Appl Phys Lett*, 97(2010) 253110; doi.org/10.1063/1.3525940.
75. Fujiwara H, Principles of Optics. In Spectroscopic Ellipsometry, (John Wiley & Sons, Ltd), 2007, pp 13
76. Fujiwara H, Data Analysis. In Spectroscopic Ellipsometry, (John Wiley & Sons, Ltd), 2007, pp 147
77. Wurstbauer U, Röling C, Wurstbauer U, Wegscheider W, Vaupel M, Thiesen P H, Weiss D, *Appl Phys Lett*, 97(2010)231901; doi.org/10.1063/1.3524226.
78. Matković A, Beltaos A, Milićević M, Ralević U, Vasić B, Jovanović D, Gajić R, *J Appl Phys*, 112(2012) 123523; doi.org/10.1063/1.4771875.
79. Yang L, Deslippe J, Park C-H, Cohen M L, Louie S G, *Phys Rev Lett*, 103(2009)186802; doi.org/10.1103/PhysRevLett.103.186802.
80. Zhou K G, Chang M J, Wang H X, Xie Y L, Zhang H L, *J Nanosci Nanotechnol*, 12(2012)508-512.

81. Nair R R, Wu H A, Jayaram P N, Grigorieva I V, Geim A K, *Science*, 335(2012)442-444.
82. Han S, Choi M Y, Kumar P, Stanley H E, *Nat Phys*, 6(2010)685-689.
83. Algara Siller G, Lehtinen O, Wang F C, Nair R R, Kaiser U, Wu H A, Geim A K, Grigorieva I V, *Nature*, 519(2015) 443-.
84. Zhou W, Yin K, Wang C, Zhang Y, Xu T, Borisevich A, Sun L, Idrobo J C, Chisholm M F, Pantelides S T, Klie R F, Lupini A R, *Nature,* 528(2015)E1-E2.
85. Sobrino Fernández Mario, M. Neek Amal, Peeters F M, *Phys Rev B,* 94(2016)045436; doi.org/10.1103/PhysRevB.94.045436.
86. Abergel D S L, Russell A, Fal'ko V I, *Appl Phys Lett*, 91(2007)063125-; doi.org/10.1063/1.2768625
87. Roddaro S, Pingue P, Piazza V, Pellegrini V, Beltram F, *Nano Lett*, 7(2007)2707-2710.
88. Sarkar B, M Sc Thesis, A Study of electronic properties of multilayer graphene under uniaxial elastic strain, Indian Institute of Technology Madras, Chennai, India, 2013.
89. Chen C F, Park C-H, Boudouris B W, Horng J, Geng B, Girit C, Zettl A, Crommie M F, Segalman R A, Louie S G, Wang F, *Nature*, 471(2011)617-620.
90. Eda G, Lin Y Y, Mattevi C, Yamaguchi H, Chen H-A, Chen I S, Chen C-W, Chhowalla M, *Adv Mater*, 22(2010) 505-509.
91. Chien C T, Chien C T, Li S S, Lai W J, Yeh Y C, Chen H A, Chen I S, Chen L C, Chen K H, Nemoto T, Isoda S, Chen M, Fujita T, Eda G, Yamaguchi H, Chhowalla M, Chen C W, *Angew Chem*, 51(2012)6662-6666.
92. Pan D, Zhang J, Li Z, Wu M, *Adv Mater*, 22(2010)734-738.
93. Xin G, Meng Y, Ma Y, Ho D, Kim N, Cho S M, Chae H, *Mat Lett*, 74(2012)71-73.
94. Zhuo S, Shao M, Lee S T, *ACS Nano*, 6(2012)1059-1064.
95. Shen J, Zhu Y, Yang X, Zong J, Zhang J, Li C, *New J Chem*, 36(2012)97-101.
96. Jin S H, Kim D H, Jun G H, Hong S H, Jeon S, *ACS Nano*, 7(2013)1239-1245.
97. Wang X, Zhi L, Müllen K, *Nano Lett*, 8(2008)323-327.
98. Wu J, Agrawal M, Becerril H A, Bao Z, Liu Z, Chen Y, Peumans P, *ACS Nano*, 4(2010)43-48.
99. Sangeeth C S S, Jaiswal M, Menon R, *J Appl Phys*, 105(2009)063713; doi.org/10.1063/1.3097759
100. Shi H, Wang C, Sun Z, Zhou Y, Jin K, Yang G, *Sci China Phys Mech Astron*, 58(2014)1-5.
101. Moon I K, Kim J I, Lee H, Hur K, Kim W C, Lee H, *Sci Rep*, 3(2013)1112;doi:10.1038/srep01112.
102. He Q, Wu S, Gao S, Cao X, Yin Z, Li H, Chen P, Zhang H, *ACS Nano*, 5(2011)5038-5044.
103. Fan J, Liu S, Yu J, *J Mater Chem*, 22(2012)17027-17036.
104. Anish Madhavan A, Kalluri S, K Chacko D, Arun T A, Nagarajan S, Subramanian K R V, Sreekumaran Nair A, Nair S V, Balakrishnan A, *RSC Adv*, 2(2012)13032-13037.
105. Chen T, Hu W, Song J, Guai G H, Li C M, *Adv Funct Mater*, 22(2012)5245-5250.
106. Zhang D W, Li X D, Li H B, Chen S, Sun Z, Yin X J, Huang S M, *Carbon*, 49(2011)5382-5388.
107. Choi H, Kim H, Hwang S, Choi W, Jeon M, *Sol Energy Mater Sol Cells*, 95(2011)323-325.
108. Lee K S, Lee Y, Lee J Y, Ahn J-H, Park J H, *Chem Sus Chem*, 5(2012)379-382.
109. Kaniyoor A, Ramaprabhu S, *J Appl Phys*, 109(2011)124308; doi.org/10.1063/1.3600231.
110. Wang J T-W, Ball J M, Barea E M, Abate A, Alexander-Webber J A, Huang J, Saliba M, Mora-Sero I, Bisquert J, Snaith H J, Nicholas R J, *Nano Lett*, 14(2014)724-730.
111. Yan K, Wei Z, Li J, Chen H, Yi Ya, Zheng X, Long X, Wang Z, Wang J, Xu J, Yang S, *Small*, 11(2015)2269-2274.
112. Wu Z, Bai S, Xiang J, Yuan Z, Yang Y, Cui W, Gao X, Liu Z, Jin Y, Sun B, *Nanoscale*, 6(2014)10505-10510.
113. You P, Liu Z, Tai Q, Liu S, Yan F, *Adv Mater*, 27(2015)3632-3638.
114. Lang F, Gluba M A, Albrecht S, Rappich J, Korte L, Rech B, Nickel N H, *J Phys Chem Lett*, 6(2015)2745-2750.
115. Han T H, Lee Y, Choi M R, Woo S H, Bae S H, Hong B H, Ahn J H, Lee T W, *Nat Photon*, 6(2012)105-110

116. Li N, Oida S, Tulevski G S, Han S J, Hannon J B, Sadana D K, Chen T C, *Nat Commun*, 4(2013)2294; doi:10.1038/ncomms3294.
117. Sun T, Wang Z L, Shi Z J, Ran G Z, Xu W J, Wang Z Y, Li Y Z, Dai L, Qin G G, *Appl Phys Lett*, 96(2010) 133301; doi.org/10.1063/1.3373855.
118. Chang J H, Lin W H, Wang P C, Taur J I, Ku T A, Chen W T, Yan S J, Wu C I, *Sci Rep*, 5(2015)9693; doi:10.1038/srep09693.
119. Tielrooij K J, Piatkowski L, Massicotte M, Woessner A, Ma Q, Lee Y, Myhro K S, Lau C N, Jarillo H P, van Hulst N F, Koppens F H L, *Nat Nano*, 10(2015)437-443.
120. Xia F, Mueller T, Lin Y-m, Valdes-Garcia A, Avouris P, *Nat Nano*, 4(2009)839-843.
121. Echtermeyer T J, Nene P S, Trushin M, Gorbachev R V, Eiden A L, Milana S, Sun Z, Schliemann J, Lidorikis E, Novoselov K S, Ferrari A C, *Nano Lett*, 14(2014)3733-3742.
122. An Y, Behnam A, Pop E, Ural A, *Appl Phys Lett*, 102(2013)013110; doi.org/10.1063/1.4773992.
123. Echtermeyer T J, Milana S, Sassi U, Eiden A, Wu M, Lidorikis E, Ferrari A C, *Nano Lett*, 16(2016)8-20.
124. Zhang H, Bao Q, Tang D, Zhao L, Loh K, *Appl Phys Lett*, 95(2009)141103; doi.org/10.1063/1.3244206.
125. Bao Q, Zhang H, Yang J-x, Wang S, Tang D Y, Jose R, Ramakrishna S, Lim C T, Loh K P, *Adv Funct Mater*, 20(2010)782-791.
126. Purdie D G, Popa D, Wittwer V J, Jiang Z, Bonacchini G, Torrisi F, Milana S, Lidorikis E, Ferrari A C, *Appl Phys Lett*, 106(2015)253101; doi.org/10.1063/1.4922397
127. Tolstik N, Sorokin E, Sorokina I T, *Opt Express*, 22(2014)5564-5571.
128. Mishra S R, Rawat H S, Mehendale S C, Rustagi K C, Sood A K, Bandyopadhyay R, Govindaraj A, Rao C N R, *Chem Phys Lett*, 317(2000)510-510-514.
129. Zhu P, Wang P, Qiu W, Liu Y, Ye C, Fang G, Song Y, *Appl Phys Lett*, 78(2001)1319; doi.org/10.1063/1.1352670
130. Haripadmam P C, Kavitha M K, John H, Krishnan B, Gopinath P, *Appl Phys Lett*,101(2012)071103; doi.org/10.1063/1.4745605.
131. Kavitha M K, Haripadmam P C, Gopinath P, Krishnan B, John H, *Mater Res Bull*, 48(2013)1967-1971.
132. Cao B, Zhang Y, Zhang H, Zhu J, *Chin Opt Lett*, 3(2005)S248-S250.
133. Kavitha M K, John H, Gopinath P, Philip R, *J Mater Chem C*, 1(2013)3669-3676.
134. Zhao M, Peng R, Zheng Q, Wang Q, Chang M J, Liu Y, Song Y L, Zhang H L, *Nanoscale*, 7(2015)9268-9274.
135. Liu Z B, Xu Y F, Zhang X Y, Zhang X L, Chen Y S, Tian J G, *J Phys Chem B*, 113(2009)9681-9686
136. Kavitha M K, Ph D Thesis, Tailoring the defects in ZnO and ZnO-graphene hybrids for visible light photoconductivity and nonlinear absorption, Indian Institute of Space Science and Technology, Thiruvananthapuram, India, 2015.

[Received: 5.2.2016]

Manu Jaiswal

Manu Jaiswal graduated from St. Stephen's College, Delhi (India) in 2001 with a degree in Physics (Hons.). He then joined the Integrated Ph D program in Physics at Indian Institute of Science, Bangalore. After completing Ph D in 2008, he worked as a post-doctoral fellow at the Max Planck Institute for Polymer Research, Mainz and subsequently at the National University of Singapore. He joined as an Assistant Professor in the Department of Physics, IIT Madras in Dec. 2011 – where he currently works on two-dimensional systems. He is a recipient of the Young Faculty Recognition Award 2016 from IIT Madras. He has also received Prof Anil Kumar Memorial award for best Ph D thesis in Physics from IISc Bangalore and Dr G C Jain Memorial award from Materials Research Society of India for best Ph D thesis in Material Science.

M K Kavitha

Ms Kavitha received her Ph D in 2015 from Indian Institute of Space Science and Technology, Thiruvananthapuram, India. During her Ph D, she worked on the synthesis of ZnO and ZnO/graphene hybrids for visible light photocurrent generation and nonlinear optical applications. Currently she works as a postdoctoral fellow at the Indian Institute of Technology Madras, Chennai, India on graphene-interfaced flexible perovskite solar cells. Her research interests include synthesis of semiconductor/graphene hybrid materials and its optical applications.